



# Molecular dynamics study of carbon dioxide and nitrogen selectivity through poly[bis((methoxyethoxy)ethoxy)phazene] (MEEP) membrane

February 2024

*Changing the World's Energy Future*

Birendra Adhikari, Hyeonseok Lee, John R Klaehn, Christopher J Orme, Aaron D Wilson, Joshua S McNally, Frederick F Stewart



**DISCLAIMER**

This information was prepared as an account of work sponsored by an agency of the U.S. Government. Neither the U.S. Government nor any agency thereof, nor any of their employees, makes any warranty, expressed or implied, or assumes any legal liability or responsibility for the accuracy, completeness, or usefulness, of any information, apparatus, product, or process disclosed, or represents that its use would not infringe privately owned rights. References herein to any specific commercial product, process, or service by trade name, trade mark, manufacturer, or otherwise, does not necessarily constitute or imply its endorsement, recommendation, or favoring by the U.S. Government or any agency thereof. The views and opinions of authors expressed herein do not necessarily state or reflect those of the U.S. Government or any agency thereof.

**Molecular dynamics study of carbon dioxide and  
nitrogen selectivity through  
poly[bis((methoxyethoxy)ethoxy)phosphazene]  
(MEEP) membrane**

**Birendra Adhikari, Hyeonseok Lee, John R Klaehn, Christopher J Orme, Aaron D  
Wilson, Joshua S McNally, Frederick F Stewart**

**February 2024**

**Idaho National Laboratory  
Idaho Falls, Idaho 83415**

**<http://www.inl.gov>**

**Prepared for the  
U.S. Department of Energy  
Under DOE Idaho Operations Office  
Contract DE-AC07-05ID14517**

# Molecular dynamics study of carbon dioxide and nitrogen selectivity through poly[bis((methoxyethoxy)ethoxy)phosphazene] (MEEP) membrane

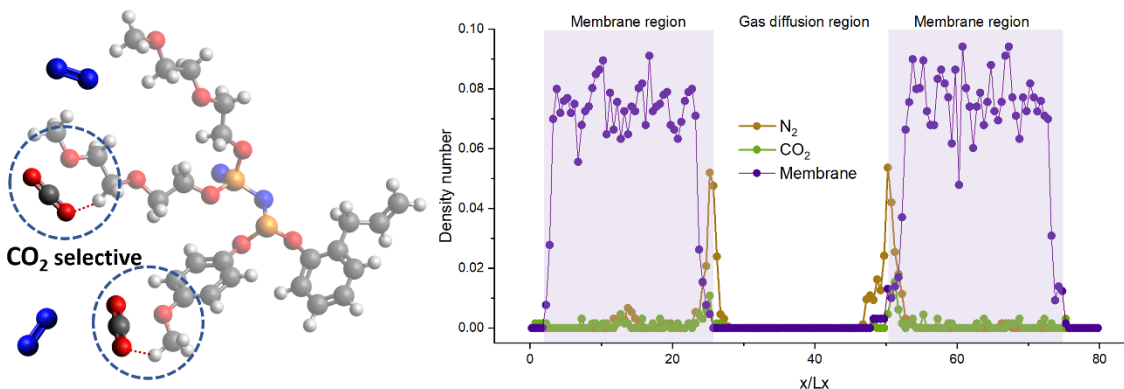
*Hyeonseok Lee, John R. Klaehn, Christopher J. Orme, Joshua S. McNally, Aaron D. Wilson,*

*Frederick F. Stewart, and Birendra Adhikari\**

Chemical Separations Group, Idaho National Laboratory, P.O. Box 1625, Idaho Falls, ID 83415-2208, USA

\*Corresponding author: [birendra.adhikari@inl.gov](mailto:birendra.adhikari@inl.gov)

## Graphical Abstract



## Highlights

- Molecular dynamics simulated CO<sub>2</sub>/N<sub>2</sub> selectivity of an amorphous poly[bis((methoxyethoxy)ethoxy)phosphazene] membrane shows good agreement with experimental results.
- The amorphous polymer membrane exhibits excellent CO<sub>2</sub> permeability and CO<sub>2</sub>/N<sub>2</sub> selectivity.
- Lewis acid–base and hydrogen bonding provide kinetic stability for gas permeation through the membrane.
- Moisture, represented by the water molecules in the feed stream, does not have a significant impact on CO<sub>2</sub> transport and selectivity over N<sub>2</sub>.

## Abstract

A molecular dynamics simulation model was developed to comprehensively understand carbon dioxide over nitrogen ( $\text{CO}_2/\text{N}_2$ ) selectivity through polyphosphazene-based membrane comprising of poly[bis((methoxyethoxy)ethoxy)phosphazene] (MEEP) selective layer at the molecular level. The effects of temperature, pressure, and initial feed gas composition on the  $\text{CO}_2$  transport on a polymer membrane were studied. The computed free energy and density profile of the permeating gas mixture exhibited that  $\text{CO}_2$  molecules express higher interactions with the membrane than  $\text{N}_2$  molecules, resulting in higher  $\text{CO}_2/\text{N}_2$  selectivity. Statistical analysis of gas molecules ( $\text{CO}_2$ , water ( $\text{H}_2\text{O}$ ), and  $\text{N}_2$ ) transportation suggested that hydro- and  $\text{CO}_2$ -philic functional groups in the membrane significantly impact  $\text{CO}_2$  permeability and  $\text{CO}_2/\text{N}_2$  selectivity. This study suggested that Lewis acid–base and hydrogen bonding combinations contribute to  $\text{CO}_2$  permeation and  $\text{CO}_2/\text{N}_2$  selectivity. An equal  $\text{CO}_2/\text{N}_2$  selectivity was observed with and without water vapor in the feed gas suggesting that water does not hinder  $\text{CO}_2$  transport through the membrane.

**Keywords:**  $\text{CO}_2$  capture,  $\text{CO}_2/\text{N}_2$  selectivity, polyphosphazene membrane, hydrogen bonding, Lewis acid–base interaction

## 1. Introduction

Climate change caused by recent global warming is one of Earth's major challenges because it has impacted every aspect of life on Earth. Extinction of several species, rising seas and oceans, and increased frequency of natural disasters such as flood, erosion, dry condition, and wildfire have been observed. Increased levels of greenhouse and industrial emissions, such as carbon dioxide (CO<sub>2</sub>), methane, ethane, SO<sub>x</sub>, and NO<sub>x</sub>, in the atmosphere are the main contributors to this ongoing crisis. These greenhouse gases trap the sunlight and make the atmosphere warmer. The Earth's average temperature has already risen by more than 2 °C in the last 50 years alone, and if this trend continues, this planet Earth will become inhabitable for human life by the year 2100 (Clark et al., 2020).

CO<sub>2</sub> is the main contributor to global warming. It accounts for a total of 72.6% of total greenhouse emissions (Wang, Xing and Shen, 2023). In the last 50 years alone, CO<sub>2</sub> level in the atmosphere has increased by 50 ppm, from 360 ppm to 418 ppm. This fast increase of CO<sub>2</sub> level in the atmosphere has never been observed in human history. At the current rate, the CO<sub>2</sub> level can reach 570 ppm in the next 75 years (Alli et al., 2023). This rate of CO<sub>2</sub> increase in the atmosphere demands proactive management of carbon emissions. Carbon capture and utilization from different point sources, such as flue gas and directly from the air, are necessary for sustainable atmospheric carbon management.

Carbon capture is the enrichment of CO<sub>2</sub> from various sources, storing it permanently or using it for enhanced oil recovery or making fuels and chemicals such as syn gas, butanol, methanol, ethanol, and dimethyl ether (Diaz et al., 2018). These processes prevent CO<sub>2</sub> from going back into the atmosphere. It may even be necessary to remove CO<sub>2</sub> from the air via direct air capture (DAC). CO<sub>2</sub> is usually captured using cryogenic capture, pressure swing adsorption,

chemical absorption, and membrane-based capture. The cryogenic process captures CO<sub>2</sub> by lowering the temperature of feed gas. CO<sub>2</sub> freezes at a temperature of ~ 195K while all other gases remain in gas form at that temperature, and as a result, CO<sub>2</sub> capture is achieved. However, to get high-purity CO<sub>2</sub> (>99.9%), a much lower temperature (115 K) is desired, and that can make cryogenic separation an energy-intensive process. In addition, cryogenic capture is usually done at a large scale, making it a capital-intensive process and unattractive for small-scale applications. Chemical absorption is the most popular form of CO<sub>2</sub> capture since many industrial capture processes use this technology for carbon capture. A chemical agent bonds with CO<sub>2</sub> in a dilute CO<sub>2</sub> gas stream under a specific pressure-temperature regime, and CO<sub>2</sub> is later released under different physical conditions, forming high-purity CO<sub>2</sub>. This carbon dioxide capture method is at an optimal technical maturity level, and various chemical agent options are commercially available. In this process, amines are often used to form soluble carbonate salts with captured CO<sub>2</sub>. Carbonation typically happens at low temperatures, from ambient temperature to 60-65 °C, and the carbonates are heated to release the captured CO<sub>2</sub>. The common types of amines are alkanolamines, such as monoethanolamine (MEA) and diglycolamine (DGA) (Al-Juaied and Rochelle, 2006). However, the capture cost is high, and the loss of capture agents is a major problem. A range of amines, including primary, secondary, and tertiary amines, have all been explored as capture agents. This includes switchable polarity tertiary amines such as 1-cyclohexylpiperidine and dimethylcyclohexylamine, which have been explored for CO<sub>2</sub> capture and as a draw solution for the forward osmosis application (Adhikari et al., 2017; Adhikari et al., 2019; Diaz et al., 2018; Klaehn et al., 2021; Lister et al., 2021; Wendt et al., 2016; Wilson et al., 2021; Wilson et al., 2022; Wilson et al., 2019). However, alkanolamines are known for their deficiencies as well. They are known for high energy usage during the solvent regeneration step.

Excessive corrosion, scale-up difficulties, and amine degradation over time are some of the known issues related to this capture process (Rochelle, 2012). These attributes make them energy-intensive, and the amount of solvent used and lost in the process makes them highly unsustainable with a large chemical footprint.

Another capture method that is explored heavily is pressure swing adsorption (PSA). PSA technology uses an adsorbent material by fluctuating the pressure to absorb and desorb CO<sub>2</sub> (Siqueira et al., 2017). Different adsorbent materials such as zeolites, metal–organic frameworks (MOFs), and activated carbon can be used as adsorbents to capture CO<sub>2</sub> (McQueen et al., 2021). CO<sub>2</sub> adsorption usually happens at an elevated pressure above 40 bar (Riboldi and Bolland, 2017; Zhao et al., 2021). The adsorbed CO<sub>2</sub> is then released (desorbed) at ambient pressure, often aided by a vacuum. A significant disadvantage of this process is that it requires a long residence time for all the sites to be filled by CO<sub>2</sub>, resulting in higher capital and energy costs. The adsorption materials lose binding efficacy over time, making them capital-intensive (Yu, Huang and Tan, 2012).

Membranes are considered a cost-effective and less energy-intensive option many applications including carbon capture (Adhikari, 2015; Adhikari et al., 2023a; Adhikari and Pellegrino, 2015; Amer, Adhikari and Pellegrino, 2011; Stickel et al., 2018; Wendt, Wahlen and Adhikari, 2022). Membranes are semi-permeable barriers for one component over the other component in the mixture gas so that a selectivity of one component over the other can be achieved. Membranes can be formed from various materials, such as polymers, ceramics, and mixed-matrix, and in various geometries, such as hollow fiber, flat sheet, and spiral wound. The transmembrane pressure gradient can drive CO<sub>2</sub> transport through the membranes. The solution diffusion model of membrane transport suggests that gas molecules dissolve in the membrane and diffuse from one

end to the other. Polymers such as polyethyleneimine (PEI), polyvinylidene fluoride (PVDF), polydimethylsiloxane (PDMS), and polyethersulfone (PES) are used as membrane materials for CO<sub>2</sub> transport membranes. Facilitation materials can be added to membrane materials to enhance CO<sub>2</sub> transport through the membrane. These facilitated materials, such as ionic-liquid gels (Lee and Gurkan, 2021), Polyvinylamine-Matrimid (Aframehr et al., 2022), have a higher affinity for CO<sub>2</sub> and transport CO<sub>2</sub> with facilitated mobile and immobile carriers. Commercial membranes were introduced two decades ago, and several commercial CO<sub>2</sub> selective membranes are now available in different membrane chemistry and module geometry. Pebax elastomers from Arkema are used in state-of-art membranes because of their high CO<sub>2</sub>/N<sub>2</sub> selectivity above 40 and CO<sub>2</sub> permeability above 100 Barrer (Bondar, Freeman and Pinnau, 2000; Liu et al., 2016). All new CO<sub>2</sub> selective membranes are often compared against Pebax or Pebax derivatives in membrane-based carbon capture.

Despite positive attributes, membrane-based CO<sub>2</sub> capture also has deficiencies. Membrane processes are capital-intensive processes with high costs of membrane material and system installation. In addition, electricity runs membrane processes, making it debatable from a sustainability standpoint. CO<sub>2</sub>/N<sub>2</sub> selectivity and CO<sub>2</sub> permeability are mutually exclusive: the higher the CO<sub>2</sub>/N<sub>2</sub> selectivity, the lower the CO<sub>2</sub> permeability, and vice-versa (Park et al., 2017). In addition, commercial membranes are known to have pinholes and deformities with declined membrane performance (Bridge et al., 2022).

Our research group at Idaho National Laboratory (INL) has explored and developed polyphosphazene gas-separation polymers. Polyphosphazene polymers contain a repeating phosphorus-nitrogen backbone with oxy- or amino-functional groups attached to phosphorus. These polymers have been demonstrated to separate O<sub>2</sub>/N<sub>2</sub> (Adhikari et al., 2021; Stewart et al.,

2021) and CO<sub>2</sub>/N<sub>2</sub> (Orme et al., 2006a; Orme, Klaehn and Stewart, 2004). Polyphosphazene polymers can range from hard, solid materials to soft gels depending on the functional groups used; however, most gas permeability research has focused on a softer polymer, such as poly[bis((2-methoxyethoxy)ethoxy)phosphazene] (MEEP, Figure 1). MEEP is a specialty polymer that can be fabricated into thin, self-healing, and defect-free membranes (Sekizkardes et al., 2021). MEEP has excellent CO<sub>2</sub>/N<sub>2</sub> selectivity above 40 and CO<sub>2</sub> permeability above 400 Barrer, matching the upper bound limits for CO<sub>2</sub>/N<sub>2</sub> separations (Robeson, 2008). A thin selective layer can be fabricated to minimize the cost of capture and energy required to drive the membrane processes.

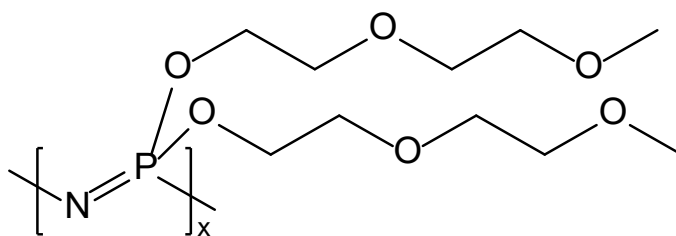


Figure 1. The chemical structure of MEEP

CO<sub>2</sub> permeability and CO<sub>2</sub>/N<sub>2</sub> selectivity are critical for efficient CO<sub>2</sub> enrichment and capture (Rafiq, Deng and Hägg, 2016). However, the science behind CO<sub>2</sub> transport through these polymers must be better understood. Computational simulation methods have been broadly utilized to understand membranes. Our team at INL is currently developing a MEEP-based membrane and focusing on a technique to develop a mixed matrix membrane to attain higher mechanical stability while capturing CO<sub>2</sub> from low-concentration CO<sub>2</sub> sources (Adhikari et al., 2023b; Nilkar et al., 2023). To better understand the mechanism of the CO<sub>2</sub>/N<sub>2</sub> selectivity through the membrane, molecular dynamics simulations (MDS) were performed in this study. Thermodynamics and kinetics of CO<sub>2</sub>, N<sub>2</sub>, and water (H<sub>2</sub>O), all gas phase molecules, were

investigated. Specific interactions, such as Lewis-acid interaction and hydrogen bonding were the focus of this study. The diffusion of CO<sub>2</sub> and N<sub>2</sub> molecules through the membrane was also studied. Temperature, pressure, and gas composition in the mixed gas were varied to explore their influence on CO<sub>2</sub>/N<sub>2</sub> selectivity and transport. This study aimed to determine the optimal process condition for the capture process using MEEP membrane for the high CO<sub>2</sub>/N<sub>2</sub> selectivity and economic and environmental sustainability.

## **2. Methods**

MDS is based on Newton's equations for classical particles, applied to macroscopic properties regarding molecular behavior from the microstate of the system. MDS calculates the motion of a collection of interacting particles by repeatedly solving the equations for long enough time steps. MDS provides an adequate level of approximation for modeling structural properties and transport motion in a membrane material. The membrane of our choice, MEEP, is a polymer with no surface charges. Thus, an electrically insulating molecular model was employed to study this polymer. This model did not require the immediate necessity of other intense methods, e.g., computational Ab initio chemistry methods. The gas particle–particle and gas particle–membrane interactions describing the motion were calculated at an adequate level of approximation using conventional force fields and parameters.

### **2.1 Poly[bis((methoxyethoxy)ethoxy)phosphazene] membrane and gas molecules**

The atom–atom interaction and several force fields were used to model the MEEP polymer structure (Allcock et al., 1999; Luther et al., 2003; Wang and Balbuena, 2004). These force fields have been shown to adequately reproduce structural and timescale correlation functions such as transition density. As illustrated in our previous work, (MEEP) was synthesized through the reaction of the sodium salt of 2-(2-methoxyethoxy)ethanol with poly[bis-(chloro)phosphazene],

showing both high CO<sub>2</sub>/N<sub>2</sub> selectivity and CO<sub>2</sub> permeability (Orme et al., 2006b; Orme et al., 2021). A molecular MEEP structure was generated. Figure 2a shows the schematic atomic representation of bis-(2-(2-methoxy)ethoxy)ethoxyphosphazene monomer structure. Based on our previous study, the molecular model of the MEEP was developed from the molecular builder and computational simulations. The all-atoms General AMBER force field (GAFF) was employed (Wang et al., 2006; Wang et al., 2004) for this membrane model with conformationally averaged AM1-BCC charges and gas molecules, CO<sub>2</sub>-N<sub>2</sub> model (Potoff and Siepmann, 2001), and TIP3P model (Price and Brooks III, 2004) water model (3 site rigid water molecular model having point charges and potential parameters assigned to each of the three atoms) were utilized. The simulated systems contain 10 MEEP chains, each 50 monomers long and terminated with hydrogen in a periodic box with a density of 1.15 g/mL (experimental density at room temperature is 1.22 g/mL) (Orme et al., 2021). The chains were then relaxed with an average temperature of 500 K for 5 ns using microcanonical dynamics. The simulation required a time step size of 0.5 fs for energy conservation. The system was initially set up with two membrane walls. The compartment between the two membranes contained the feed molecules, while the two outer compartments initially represented a vacuum, serving as the driving force for the simulation. We chose this configuration because of the periodic boundary conditions in our simulation, which offers advantages in setting up the initial simulation and ensuring efficient execution.

## **2.2 Simulation methods and validation**

The MDS technique was used to describe several structural (gas molecules–polymer membrane coordination, membrane configuration, and system morphology) and thermodynamics and kinetics properties. MDS was performed to evolve the equation of motion with the Large-scale Atomic/Molecular Massively Parallel Simulator (LAMMPS) simulation package (Thompson et

al., 2022a) in a three-dimensional simulation box with periodic boundary conditions imposed in all directions. The initial non-overlapping liquid-like random molecular configurations were constructed by the software package PACKMOL (Martínez et al., 2009). The system was allowed to equilibrate for a period of 5 ns with integration using a Nose–Hoover thermostat and barostat, where the system's density converged to a mean value corresponding to temperature and pressure conditions. The Lennard-Jones (LJ) and Coulomb interactions were modeled using a cutoff distance of 1.4 nm. LJ potentials describe the potential energy of interaction between nonbonding particles as a function of their separation distance. The long-range Coulombic interactions (beyond the 1.4 nm cutoff) were computed using the particle-particle-particle–mesh (PPPM) (Hockney and Eastwood, 1989) with an accuracy of  $10^{-4}$ . The Lorentz-Berthelot combining rule is used in the applied force field. The production simulations were performed for 10 ns, while the temperature and pressure were maintained constant by a coupled thermostat and a barostat. These were monitored and controlled as part of the simulation setup. The molecular trajectories were sampled every 1,000 steps to enable the calculation of desired parameters.

As the first step, calculations to validate the system that describes both structural and dynamic properties were performed. Figure 2b compares the computed and experimental CO<sub>2</sub>/N<sub>2</sub> selectivity values (Jha and Way, 2008; Orme et al., 2021). In our study, we considered pure CO<sub>2</sub> and N<sub>2</sub> feed gas to determine selectivity. The simulation allowed us to calculate the number of gas molecules or moles that permeated through the membrane, enabling us to calculate selectivity. An acceptable correlation between the trends in experiments and computer simulations is expected for the selected force field. The simulation results confirmed the validity of the model developed. Hydrogen bonds were constrained and determined using distance and angle information related to CO<sub>2</sub> and oxygen atoms in the functional group.

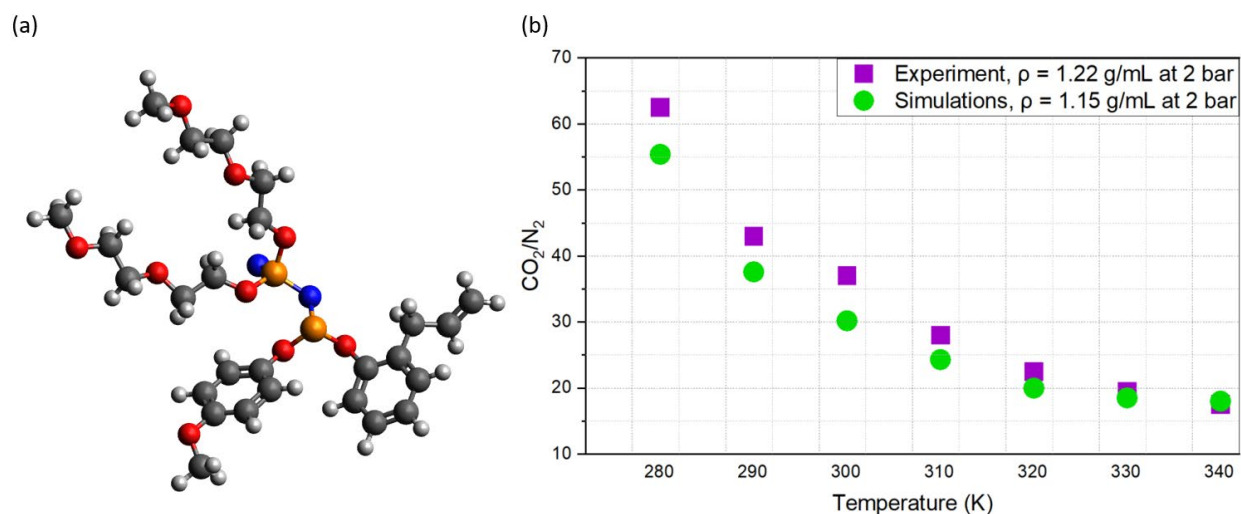


Figure 2. (a) Schematic representation of monomer for [bis-(2-(2-methoxy)ethoxy)ethoxyphosphazene], and (b)  $\text{CO}_2/\text{N}_2$  selectivity validating the model by the experimental observations.

Considering the potential mean force (PMF) underlying the translocation of gas molecules across the membrane, the Adaptive Biasing Forces (ABF) method (Fiorin, Klein and Hénin, 2013; Thompson et al., 2022b) was employed using as a collective variable, the difference between two distances. The free-energy profiles were determined by the integration of the average force exerted along the transition coordinates (Darve and Pohorille, 2001; Darve, Rodríguez-Gómez and Pohorille, 2008), defined as the projection to the x-direction separating the center of mass of gas molecules from that of the membrane. The total permeation pathway spanned 16 Å. Initially, 1 ns equilibration in the isobaric–isothermal ensemble was performed before Steered Molecular Dynamics (SMD) simulations, in which gas molecules were pulled from  $z = 16$  to 0 Å across the membrane, resulting in a total simulation time of 100 ns.

### 3. Results and Discussions

The statistics of CO<sub>2</sub> molecular motion as a function of its coordination through the amorphous membrane in the presence of N<sub>2</sub> were investigated in this study. The role of oxygen atoms bonded to a carbon atom was also studied. These carbon atoms are bonded to a methyl/ethyl/aromatic group and are the polymer's ether functional groups. The influence of several factors, such as temperature, pressure, and gas composition, on the system was studied, illustrating the thermodynamics and kinetics characteristics.

#### 3.1 Gas molecules translocation, free energy, and hydrogen bond

MDS enables an estimation of the permeability of several gases of choice (N<sub>2</sub>, CO<sub>2</sub>, H<sub>2</sub>O) and the selectivity of one gas over the other through the membrane. We first calculated the PMF for single gas molecule (N<sub>2</sub>, CO<sub>2</sub>, H<sub>2</sub>O) permeation through the membrane and later simulated the diffusion of multiple gas molecules. Calculations consist of (i) using the ABF technique for free energy difference between the physical state of the system in LAMMPS (Fiorin, Klein and Hénin, 2013; Thompson et al., 2022b), (ii) simulating motion/diffusion of gas molecules, and (iii) hydrogen bonding generation to investigate the permeability of gas molecules and CO<sub>2</sub>/N<sub>2</sub> selectivity.

The free energy profiles for gas permeation through the membrane were calculated, and the energy difference between the gas phase and diffused molecules in the membrane was determined at the center ( $x = 16 \text{ \AA}$ ). In Figure 3, two regions of the PMFs are illustrated: the barrier region centered at  $x = 16 \text{ \AA}$  and the interfacial valley around  $x = 7.8 \text{ \AA}$  (surface region). The interfacial valley region illustrates the membrane–gas phase interface, corresponding to the local free-energy minima in the PMFs. This suggests that the most favorable location for gas molecules

is near the gas molecule–membrane interface, as illustrated by the gas molecule distribution profile of Figure 3.

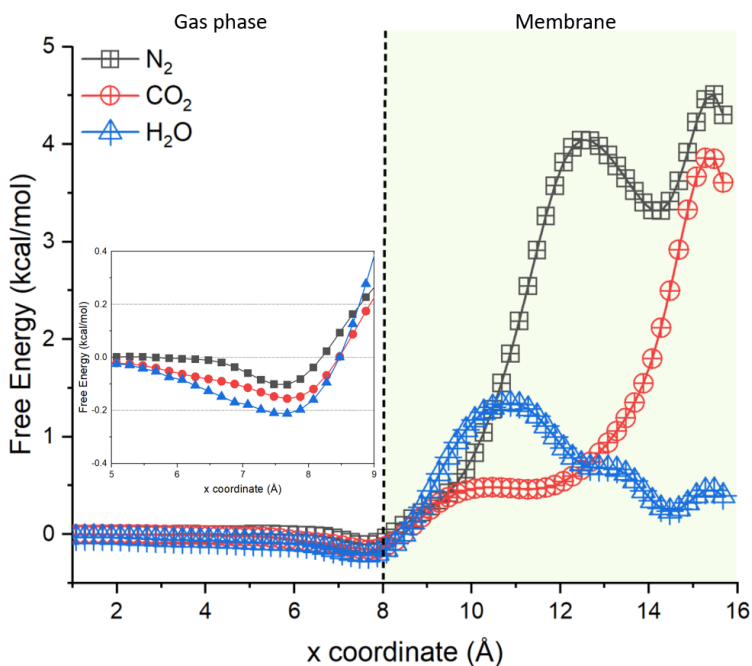


Figure 3. Free energy as a function of position with respect to the central plane of membrane polymer. Permeation of small molecules (H<sub>2</sub>O, CO<sub>2</sub>, and N<sub>2</sub>) through the membrane shows different mobility.

PMF shows 1.5 kcal/mol energy barriers against H<sub>2</sub>O permeation in Figure 3. The energy barriers of CO<sub>2</sub> and N<sub>2</sub> permeations range from 4 to 4.6 kcal/mol, respectively. These values indicate that the membrane does not present a high barrier against the permeation of H<sub>2</sub>O. In other words, the membrane is hydrophilic. While CO<sub>2</sub> and N<sub>2</sub> have barriers of similar height, the number of barriers and width are markedly different between these two elements. For instance, the free energy against CO<sub>2</sub> shows the narrowest barrier, around 2 Å away from the center with the lower height (4 kcal/mol), whereas N<sub>2</sub> has double barrier peaks and a higher barrier (4.6 kcal/mol). Apart from the barrier regions in the PMFs, interfacial valleys were observed at the membrane–gas

molecule interface (surface region), which signifies the permeation of gas molecules across the membrane. CO<sub>2</sub> corresponds to an interfacial valley of -0.15 kcal/mol, nearly 50 % lower than N<sub>2</sub>. Furthermore, the interfacial valley with H<sub>2</sub>O is the deepest ( $\approx$ -0.2 kcal/mol). This suggests that H<sub>2</sub>O is highly favorable to diffuse into the interface region. However, water does not weaken the transport of either CO<sub>2</sub> or N<sub>2</sub>. Considering the competitive diffusion of CO<sub>2</sub> and N<sub>2</sub> in the system, shown in Figure 4, CO<sub>2</sub> is mainly observed on the membrane region of the model, whereas N<sub>2</sub> is detected on both the bulk and surface of the model due to weaker interactions with the membrane. CO<sub>2</sub> expresses higher interactions with membrane pore surfaces than N<sub>2</sub>, thus occupying available spaces and sites on the membrane surface. This would result in a decrease of other gases being adsorbed on the membrane surface, resulting in higher permeability of CO<sub>2</sub> through the membrane.

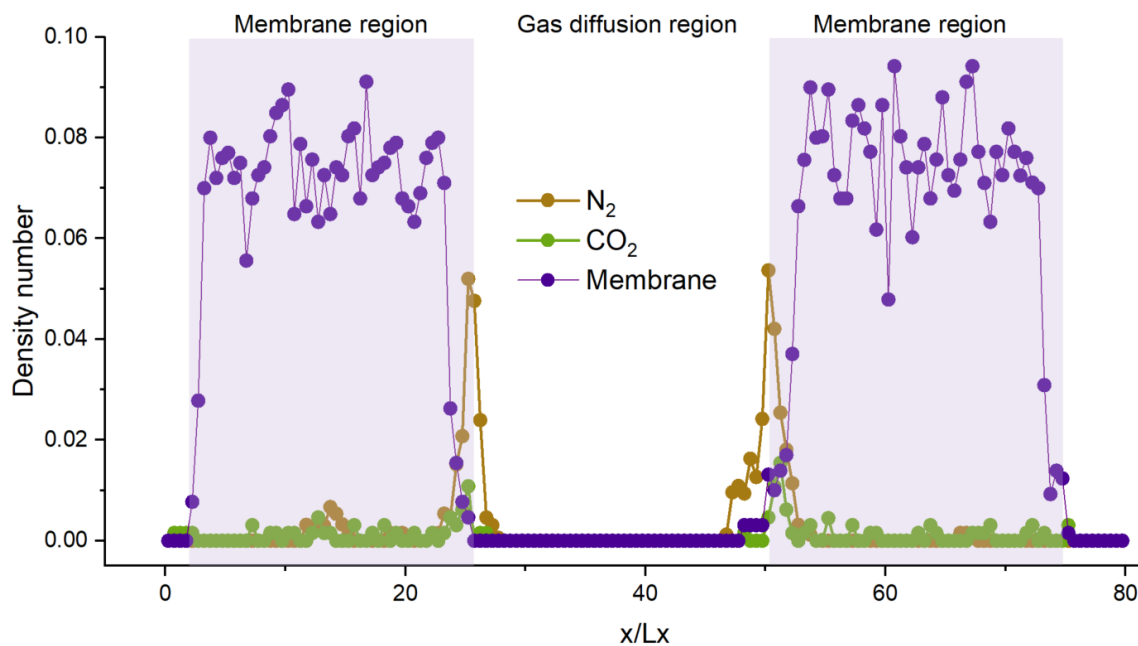


Figure 4. Density mass profile for CO<sub>2</sub> and N<sub>2</sub> at 303 K and 1 bar in a steady-state simulation and an initial solution concentration of 50:50 CO<sub>2</sub>/N<sub>2</sub> mol %. L<sub>x</sub> is the system dimension perpendicular to the membrane model.

The total dipole moment for CO<sub>2</sub> is zero. However, it has an electric quadrupole moment (Buckingham and Disch, 1963; Kauffman, 2001). The bond electron density of CO<sub>2</sub> is more polarized toward the oxygen atoms, inducing a partial positive charge on the carbon atom and a partial negative charge on the two oxygen atoms. The electron-deficient carbon atom and two oxygen atoms tend to act as Lewis acid and Lewis-base moieties, respectively (Bell et al., 2003). This makes the carbon atom an electron acceptor in a Lewis acid-base interaction with oxygen atoms in functional groups of the membrane structure. Thus, a higher selectivity of CO<sub>2</sub> over other molecules can be observed, including that of N<sub>2</sub>. It is because of its relative particle-particle interaction with other gas molecules and the interactions between CO<sub>2</sub> and CO<sub>2</sub>-philic functional groups (Di Noto et al., 2011; Raveendran and Wallen, 2002; Sergei G. Kazarian, 1996; Zhu and Baker, 2014). This Lewis acid-base mechanism can also transport protic solvents like H<sub>2</sub>O via an even stronger interaction (Nelson and Borkman, 1998; Raveendran and Wallen, 2002).

Figure 5 displays the number of hydrogen bonds as a function of the simulation timesteps while single CO<sub>2</sub> and H<sub>2</sub>O permeate the amorphous membrane, as discussed in the Method section. The number of hydrogen bonds was obtained based on geometric limitations regarding the oxygen atom in CO<sub>2</sub> as an electron acceptor associated with a Lewis acid-Lewis base interaction between CO<sub>2</sub> and the Lewis base system (ether functional group). Raveendran and Wallen demonstrate the importance of CO<sub>2</sub>-Lewis base interaction in CO<sub>2</sub> binding to functional groups based on the results of Ab initio calculations (Raveendran and Wallen, 2002). As CO<sub>2</sub> associated nonclassical hydrogen bond configuration (C-H...O)(Johnston and Cheong, 2013), the distance between carbon atom in CO<sub>2</sub> and hydrogen in organic substituent (-CH<sub>3</sub>, =CH<sub>2</sub>, and ≡CH) is limited to 2.5 to 2.95 Å, while C=O...O angle is 110 to 132 degrees. Otherwise, the number of water-associated

hydrogen bonds is calculated as an angle of 150 to 170 degrees and a distance of 1.7 to 2 Å (Rablen, Lockman and Jorgensen, 1998).

The number of hydrogen bonding between CO<sub>2</sub> and ether functional group was observed to increase at the beginning of the permeation (at the interfacial region) and then stayed constant. This implies that the ether functional groups are attracted to CO<sub>2</sub> through hydrogen bonding and are also involved in Lewis acid–base interactions. At the molecular level, this interaction could potentially serve as the dominant driving force, leading to a higher selectivity of CO<sub>2</sub> and H<sub>2</sub>O. This selectivity matches well with previously reported results (Yin et al., 2021). H<sub>2</sub>O interacts with the functional group's oxygen atom, forming a continuous hydrogen bond network based on experimental results and computational simulations (Chen et al., 2010; Ohto et al., 2015). As a result of the kinetics of steady hydrogen bond formation, complex formation between CO<sub>2</sub> and the functional group was driven by both electrostatic interactions and hydrogen bonding. It is important to note that dipole-quadrupole interactions can be regarded as a subset of electrostatic interactions due to their dependence on the electrostatic potential resulting from the combination of a permanent dipole moment and a molecular quadrupole moment.

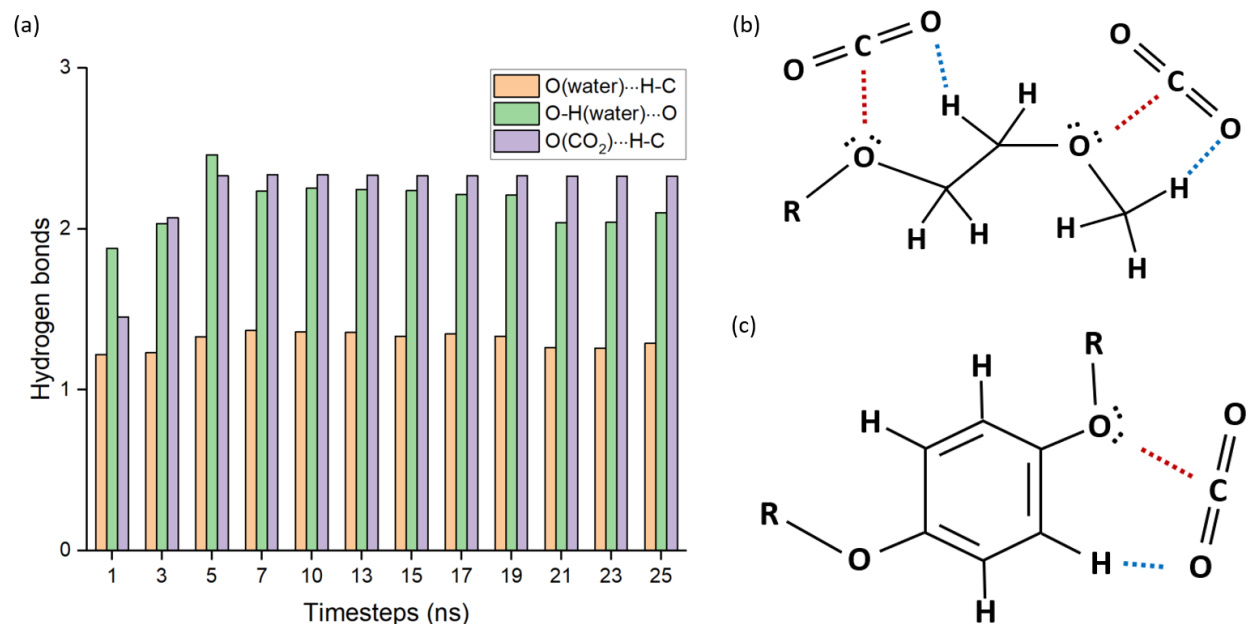


Figure 5. (a) Number of hydrogen bonds calculated; O–H(water)  $\cdots$  O (functional group), O(water)  $\cdots$  organic substituent ( $-\text{CH}_3$ ,  $=\text{CH}_2$ , and  $\equiv\text{CH}$ ), and O (CO<sub>2</sub>)  $\cdots$  organic substituent. The distance and angle limitations are based on the complexity of the H<sub>2</sub>O/CO<sub>2</sub>–Lewis base. (b–c) Schematic representations showing CO<sub>2</sub> hydrogen bond associated with CO<sub>2</sub>–Lewis base interactions in the membrane structure. Blue dots indicate hydrogen bonds and red dots show Lewis acid-base interactions.

To understand the interactions during the gas permeation process through the membrane, we conducted a study of the statistical coordination of gas molecules by the oxygen atoms of the membrane's ether functional groups. As electrostatic interactions and hydrogen bonding were considered, oxygen atom-related coordination was computed from the functional groups found within a shell of distance in three dimensions up to 8 Å centered on each gas molecule. Statistical coordination was calculated in histogram form by uniform-size binning pairwise distances from zero to the cutoff defined by the force field. Figure 6a shows the relative contribution to the

coordination of oxygen atoms as a function of the coordination bin of gas molecules. The substantial number of oxygen atom coordination by  $N_2$  was observed in 5 to 8 coordination bins, while smaller coordination numbers with  $CO_2$  and  $H_2O$  were shown within these bins. When oxygen atoms were considered, stronger interactions were observed between  $CO_2$  and  $H_2O$ . The oxygen atom plays the role of the Lewis base in the coordination calculations. Approximately 45% more total oxygen atom coordination numbers by  $CO_2$  were found than that of  $H_2O$  within 5 coordination bins, which was more tightly captured. Partially negatively charged oxygen atoms from functional groups strongly attract two partially positive hydrogen atoms in  $H_2O$ . The carbon atom in  $CO_2$  tends to be more weakly associated with the oxygen atoms in the membrane than  $H_2O$ . However,  $N_2$  undergoes weak interactions while it diffuses in the membrane structure, based on Figure 6a. These results illustrate that, within 8 coordination bins of  $N_2$ , around 50 % more oxygen atoms are present in the membrane, as it is not as strongly associated with the membrane's oxygen atom as in  $CO_2$  and  $H_2O$ .

This study illustrates in Figure 6b the average intermolecular distance between gas molecules and oxygen atoms within membrane's ether functional groups upon considering the oxygen atom coordination number in the membrane. The distribution of gas molecules neighboring the functional groups was estimated by combining the average distance with the oxygen atom contribution of coordination number. The  $H_2O$  and  $CO_2$  are mainly coordinated by single and three oxygen atoms in the functional group, respectively, supporting the previously stated assessment in Figure 6a. Otherwise,  $N_2$  exhibited a relatively linear increase in the average distance as a function of the oxygen atom coordination number. This shows that  $N_2$  is not associated with oxygen atoms in functional groups. In  $H_2O$  distribution, the difference in the average distance between a single

and two oxygen atoms is 1.45 Å. It decreases to around 0.9 Å as calculated with two and three oxygen atoms.

Regarding the following oxygen atom coordination number, the differences are constant (0.5 Å). CO<sub>2</sub> distribution results display 1.2 Å difference in the first two average distances, then decreases to 1 Å and 0.9 Å in the next 3 oxygen atom coordination numbers, respectively. A smaller difference (around 0.4 Å) was steadily estimated in the following four coordination numbers. In addition to the steady formation of hydrogen bonding, oxygen-related coordination during the gas permeation supports the formation of electrostatic interaction in the complex system.

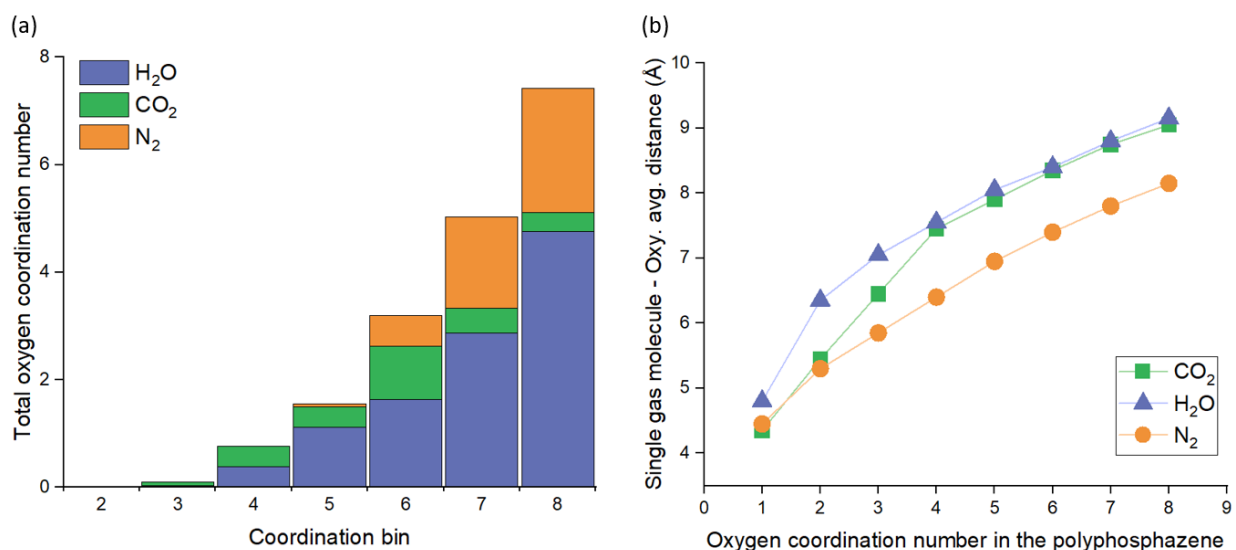


Figure 6. (a) Total coordination of gas molecules (CO<sub>2</sub>, N<sub>2</sub>, H<sub>2</sub>O) by oxygen atoms in membrane and (b) average distance (angstrom) between gas molecules and oxygen atoms of the membrane. Statistical coordination is calculated in histogram form by uniform-size binning pairwise distances from zero to the cutoff defined by the force field.

### 3.2 CO<sub>2</sub> capture application and CO<sub>2</sub> selectivity over N<sub>2</sub> in operational conditions

Figure 7 displays the simulated selective permeance of CO<sub>2</sub> over N<sub>2</sub> through the membrane as a function of the initial CO<sub>2</sub> mole fraction at different system temperatures and pressures. This analysis can identify operational conditions most selective for CO<sub>2</sub> and the molecular mechanism for transport through the membrane. These simulated temperatures were selected to explain the effects of temperature on such operations (303 K and 333 K) at constant pressure (5 bar). When the system temperature increased, the membrane demonstrated lower CO<sub>2</sub> selectivity over the feed gas's initial CO<sub>2</sub>/N<sub>2</sub> range (0.2–0.8). More specifically, the CO<sub>2</sub>/N<sub>2</sub> selectivity at 303 K is higher than at 333 K, keeping the pressure constant. When the temperature was 303 K, the CO<sub>2</sub> mole fraction in permeate gas was at least 0.8 and increased with elevated initial CO<sub>2</sub> concentration in the feed gas. Apart from the 303 K system, higher CO<sub>2</sub> mole fraction differences at 333 K by initial CO<sub>2</sub>/N<sub>2</sub> concentration were observed. An initial CO<sub>2</sub> mole fraction of 0.2 in the feed gas resulted in a permeate CO<sub>2</sub> mole fraction of 0.52, while an initial CO<sub>2</sub> mole fraction of 0.5 in the feed gas resulted in a 0.94 CO<sub>2</sub> mole fraction in the permeate. Directional Lewis acid-base interactions are the dominant driving force for this observed selectivity. Such directional bonding is inherently entropically sensitive with larger  $\Delta S$  values than systematic interactions (Stone et al., 2013a; Stone et al., 2013b; Wilson and Stewart, 2013). As temperature increases, the prevalence of directional bonds decreases. Increased temperature leads to weaker hydrogen bonding or fewer hydrogen bonds (Dougherty, 1998). This mechanism of breaking hydrogen bonds is the basis of water becoming more non-polar as temperature increases. An increase in temperature results in the weakening of hydrogen bonds and a reduction in the number of hydrogen bonds (Dougherty, 1998). This result is attributed to the mechanism of hydrogen bond breaking, which forms the basis of water's increased non-polarity at higher temperature. However, complications arising from hydrogen bond networks in membrane structure hinder the understanding of changes in hydrogen

bond dynamics. Hence, in this case of CO<sub>2</sub>, nonclassical hydrogen bond donor configuration could vary regarding gas molecule transportation and permeation. Based on the results obtained in Figure 6a, less direction bonding (dipole-quadrupole interactions) is expected at higher temperature, leading to less CO<sub>2</sub> selectivity.

At a constant temperature of 303 K, the selectivity of CO<sub>2</sub> does not significantly depend on pressure changes once the system reaches equilibrium. The highest mole fraction of CO<sub>2</sub> in the permeated gas (maximum range of 0.95 to 0.96) is found at the highest CO<sub>2</sub> concentration (0.8-mole fraction) across all pressure ranges (5 to 25 bar), with slightly higher CO<sub>2</sub> mole fraction observed at lower pressures. In the barostatting system within the 10 to 25 bar range, an increase in the initial mole fraction of CO<sub>2</sub> (from 0.2 to 0.5) did not support an increase in CO<sub>2</sub> selectivity and nearly converged to  $\pm 0.3$ . Simulation results indicate that when the initial mole fraction of CO<sub>2</sub> exceeds 0.5, the presence of a majority of CO<sub>2</sub> has a more positive impact on selectivity than when N<sub>2</sub> concentration is higher than that of CO<sub>2</sub>. Therefore, it can be concluded that the initial concentration of the gas mixture plays a significant role in CO<sub>2</sub>/N<sub>2</sub> selectivity, which can lead to variations in sequestration and capture outcomes.

To understand CO<sub>2</sub>/N<sub>2</sub> selectivity, diffusion of a mixture of gases (CO<sub>2</sub> and N<sub>2</sub>) was measured at different operating conditions, including variations in temperature, pressure, and feed composition. This enabled us to predict diffusion equilibria for the CO<sub>2</sub>/N<sub>2</sub>:50/50 mixtures. The selectivity of molecules in the system was primarily based on the hydrogen bonding and electrostatic interactions between gas molecules and the membrane structure. However, these factors may only partially account for the diffusion and permeation of molecules. In Figure 2, it was found that when a CO<sub>2</sub>-containing gas mixture diffused in the membrane, the interaction between the membrane and gas molecules would vary. Considering the competitive permeation of

CO<sub>2</sub> and N<sub>2</sub> gas molecules in the system, CO<sub>2</sub> has the dominant presence on the surface region of the membrane, whereas N<sub>2</sub> was observed both in bulk and on the surface of the membranes due to weaker interactions with the functional groups of the membrane. As discussed above, CO<sub>2</sub> expresses higher interaction with the functional groups than N<sub>2</sub>, which makes these membranes applicable for CO<sub>2</sub> capture.

### **3.3 Effect of the presence of moisture in the feed gas mixture**

The selectivity of CO<sub>2</sub> over N<sub>2</sub> can be attributed to differences in their molecular interaction, as previously discussed. This study further confirms the high selectivity of CO<sub>2</sub> over N<sub>2</sub>, even in the presence of high moisture levels (up to 0.002 water mole fraction). The permeability of water through membranes is higher than that of CO<sub>2</sub> and N<sub>2</sub>, as water molecules are more strongly attracted to membrane surfaces and diffuse more efficiently through membranes. However, we observed that water permeation did not significantly impact the ability of CO<sub>2</sub> to diffuse through the membrane selectively. Gas separation factors remained constant across a range of water mole fractions and temperatures, as shown in Figure 7d. The observed changes in gas separation factors in the presence of moisture were small, with deviations of approximately  $\pm 4\%$  at 303 K and  $\pm 7\%$  at 333 K compared to the dry condition. This suggests that the selectivity of CO<sub>2</sub> over N<sub>2</sub> remains constant for various industrial and environmental applications, even in the presence of moisture.

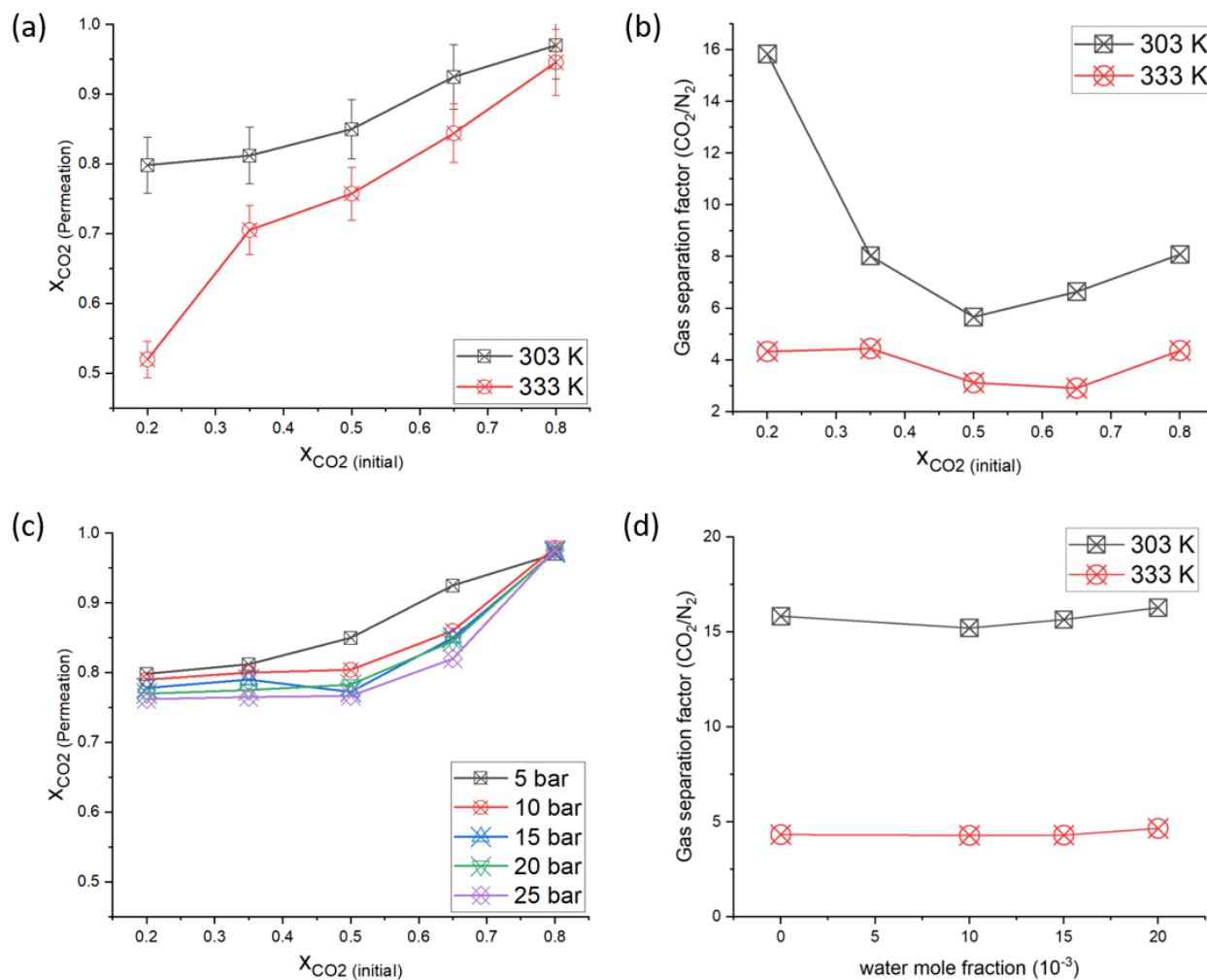


Figure 7. (a) CO<sub>2</sub> mole fraction in the permeate gas at different temperatures and 5 bar feed-side pressure, (b) CO<sub>2</sub>/N<sub>2</sub> separation factor at different temperatures and 5 bar feed-side pressure, (c) CO<sub>2</sub> mole fraction in the permeate gas at different feed-side pressure and 303 K feed-side temperature, and (d) CO<sub>2</sub>/N<sub>2</sub> separation factor at different temperatures and water mole fraction from zero to saturation.

#### 4. Conclusion

The molecular transport of CO<sub>2</sub>, N<sub>2</sub>, and H<sub>2</sub>O through the membrane under different temperature and pressure regimes was investigated by analyzing the thermodynamics of functional

group interactions. While our study did not directly address macroscopic kinetics, it provides insights into the underlying factors that govern the transport of molecules across the membrane. Considering the CO<sub>2</sub>/N<sub>2</sub> selectivity, the hydrogen bonding associated with Lewis-base interaction by the complex formation between the gas molecule and the functional group of the membrane was investigated. When the binding combinations of Lewis acid–base and hydrogen bonding dictate the gas diffusion, these are CO<sub>2</sub>/N<sub>2</sub> selectivity determinants. Also, the diffusion of CO<sub>2</sub> and N<sub>2</sub> through the membrane displays that high CO<sub>2</sub> selective permeation is confirmed, showing the applicability for separating the mixture of gases (CO<sub>2</sub> and N<sub>2</sub>) via molecular simulations under the process conditions (temperature, pressure, and gas composition). This study also confirms that the selectivity of CO<sub>2</sub>/N<sub>2</sub> is not affected by moisture in the feed gas, although the membrane is highly selective to water, which does not hinder CO<sub>2</sub>/N<sub>2</sub> selectivity. This work supports a theoretical framework to interpret those results and help uncover structure–selectivity relationships in the gas molecule–membrane complexes.

## **5. Author Contributions**

**H. Lee:** Conceptualization, Computation, Formal Analysis, Writing – Original Draft; **J. R. Klaehn, C. J. Orme, J. S. McNally, A. D. Wilson, F. F. Stewart:** Writing – Review and Editing; **B. Adhikari:** Conceptualization, Formal Analysis, Writing – Review and Editing

## **6. Competing interests**

The authors declare no competing interests.

## **7. Acknowledgment**

This manuscript has been authored by Battelle Energy Alliance, LLC (Idaho National Laboratory) under Contract No. DE-AC07-05ID14517 through the Department of Energy via the

Laboratory Directed Research and Development (LDRD) program. The views expressed in the article do not necessarily represent the views of the U.S. Department of Energy or the United States Government. The U.S. Government retains and the publisher, by accepting the article for publication, acknowledges that the U.S. Government retains a nonexclusive, paid-up, irrevocable, worldwide license to publish or reproduce the published form of this work, or allow others to do so, for U.S. Government purposes.

## References

- Adhikari, B., 2015. Separation challenges and optimizations of sustainable algae and lignocellulose based biofuels, Mechanical Engineering. University of Colorado Boulder, Boulder, CO, p. 244.
- Adhikari, B., Chowdhury, N.A., Diaz, L.A., Jin, H., Saha, A.K., Shi, M., Klaehn, J.R., Lister, T.E., 2023a. Electrochemical leaching of critical materials from lithium-ion batteries: A comparative life cycle assessment. *Resources, Conservation and Recycling* 193, 106973.
- Adhikari, B., Jones, M.G., Orme, C.J., Wendt, D.S., Wilson, A.D., 2017. Compatibility study of nanofiltration and reverse osmosis membranes with 1-cyclohexylpiperidinium bicarbonate solutions. *Journal of Membrane Science* 527, 228-235.
- Adhikari, B., Orme, C.J., Jones, M.G., Wendt, D.S., Mines, G.L., Wilson, A.D., 2019. Diffusion membrane generation of 1-cyclohexylpiperidinium bicarbonate. *Journal of Membrane Science* 583, 258-266.
- Adhikari, B., Orme, C.J., Klaehn, J.R., Stewart, F.F., 2021. Technoeconomic analysis of oxygen-nitrogen separation for oxygen enrichment using membranes. *Separation and Purification Technology* 268, 118703.
- Adhikari, B., Orme, C.J., Stetson, C., Klaehn, J.R., 2023b. Techno-economic analysis of carbon dioxide capture from low concentration sources using membranes. *Chemical Engineering Journal* 474, 145876.
- Adhikari, B., Pellegrino, J., 2015. Life-cycle assessment of five microalgae-to-biofuels processes of varying complexity. *Journal of Renewable and Sustainable Energy* 7.
- Aframehr, W., Molki, B., Bagheri, R., Sarami, N., 2022. Capturing CO<sub>2</sub> by a Fixed-Site-Carrier Polyvinylamine-/Matrimid-Facilitated Transport Membrane. *ACS Applied Polymer Materials* 4, 3380-3393.
- Al-Juaied, M., Rochelle, G.T., 2006. Absorption of CO<sub>2</sub> in Aqueous Diglycolamine. *Industrial & Engineering Chemistry Research* 45, 2473-2482.
- Allcock, H.R., Napierala, M.E., Olmeijer, D.L., Best, S.A., Merz, K.M., 1999. Ionic Conduction in Polyphosphazene Solids and Gels: <sup>13</sup>C, <sup>31</sup>P, and <sup>15</sup>N NMR Spectroscopy and Molecular Dynamics Simulations. *Macromolecules* 32, 732-741.
- Alli, Y.A., Oladoye, P.O., Ejeromedoghene, O., Bankole, O.M., Alimi, O.A., Omotola, E.O., Olanrewaju, C.A., Philippot, K., Adeleye, A.S., Ogunlaja, A.S., 2023. Nanomaterials as catalysts for CO<sub>2</sub> transformation into value-added products: A review. *Science of The Total Environment* 868, 161547.
- Amer, L., Adhikari, B., Pellegrino, J., 2011. Technoeconomic analysis of five microalgae-to-biofuels processes of varying complexity. *Bioresource Technology* 102, 9350-9359.
- Bell, P.W., Thote, A.J., Park, Y., Gupta, R.B., Roberts, C.B., 2003. Strong lewis acid– Lewis base interactions between supercritical carbon dioxide and carboxylic acids: effects on self-association. *Ind. Eng. Chem. Res.* 42, 6280-6289.
- Bondar, V.I., Freeman, B.D., Pinnau, I., 2000. Gas transport properties of poly(ether-b-amide) segmented block copolymers. *Journal of Polymer Science Part B: Polymer Physics* 38, 2051-2062.

Bridge, A.T., Pedretti, B.J., Brennecke, J.F., Freeman, B.D., 2022. Preparation of defect-free asymmetric gas separation membranes with dihydrolevoglucosenone (Cyrene™) as a greener polar aprotic solvent. *Journal of Membrane Science* 644, 120173.

Buckingham, A., Disch, R.-L., 1963. The quadrupole moment of the carbon dioxide molecule. *Proc. R. Soc. A: Math. Phys. Eng. Sci.* 273, 275-289.

Chen, X., Hua, W., Huang, Z., Allen, H.C., 2010. Interfacial water structure associated with phospholipid membranes studied by phase-sensitive vibrational sum frequency generation spectroscopy. *Journal of the American Chemical Society* 132, 11336-11342.

Clark, M.A., Domingo, N.G.G., Colgan, K., Thakrar, S.K., Tilman, D., Lynch, J., Azevedo, I.L., Hill, J.D., 2020. Global food system emissions could preclude achieving the 1.5°C and 2°C climate change targets. *Science* 370, 705-708.

Darve, E., Pohorille, A., 2001. Calculating free energies using average force. *J. Chem. Phys.* 115, 9169-9183.

Darve, E., Rodríguez-Gómez, D., Pohorille, A., 2008. Adaptive biasing force method for scalar and vector free energy calculations. *J. Chem. Phys.* 128, 144120.

Di Noto, V., Vezzu, K., Giffin, G.A., Conti, F., Bertucco, A., 2011. Effect of high pressure CO<sub>2</sub> on the structure of PMMA: a FT-IR study. *J. Phys. Chem. B* 115, 13519-13525.

Diaz, L.A., Gao, N., Adhikari, B., Lister, T.E., Dufek, E.J., Wilson, A.D., 2018. Electrochemical production of syngas from CO<sub>2</sub> captured in switchable polarity solvents. *Green Chemistry* 20, 620-626.

Dougherty, R.C., 1998. Temperature and pressure dependence of hydrogen bond strength: A perturbation molecular orbital approach. *J. Chem. Phys.* 109, 7372-7378.

Fiorin, G., Klein, M.L., Hénin, J., 2013. Using collective variables to drive molecular dynamics simulations. *Molecular Physics* 111, 3345-3362.

Hockney, R., Eastwood, J., 1989. The particle-mesh force calculation. *Computer Simulation Using Particles*, Adam Hilger, Bristol and New York, NY, USA, 120-165.

Jha, P., Way, J.D., 2008. Carbon dioxide selective mixed-matrix membranes formulation and characterization using rubbery substituted polyphosphazene. *J. Membr. Sci.* 324, 151-161.

Johnston, R.C., Cheong, P.H.-Y., 2013. C-H...O non-classical hydrogen bonding in the stereomechanics of organic transformations: theory and recognition. *Organic & Biomolecular Chemistry* 11, 5057-5064.

Kauffman, J.F., 2001. Quadrupolar solvent effects on solvation and reactivity of solutes dissolved in supercritical CO<sub>2</sub>. *J. Phys. Chem. A* 105, 3433-3442.

Klaehn, J.R., Orme, C.J., Wilson, A.D., Adhikari, B., Stewart, F.F., Snyder, S.W., 2021. Thermally reflective membrane apparatuses, and related fluid treatment systems and methods. *US Patent App.* 17/009,421.

Lee, Y.-Y., Gurkan, B., 2021. Graphene oxide reinforced facilitated transport membrane with poly(ionic liquid) and ionic liquid carriers for CO<sub>2</sub>/N<sub>2</sub> separation. *Journal of Membrane Science* 638, 119652.

Lister, T.E., Dufek, E.J., Wilson, A.D., Diaz Aldana, L.A., Adhikari, B., Gao, N., 2021. Methods and systems for the electrochemical reduction of carbon dioxide using switchable polarity materials. *US Patent* 10,975,477.

Liu, J., Hou, X., Park, H.B., Lin, H., 2016. High-Performance Polymers for Membrane CO<sub>2</sub>/N<sub>2</sub> Separation. *Chemistry – A European Journal* 22, 15980-15990.

Luther, T.A., Stewart, F.F., Budzien, J.L., LaViolette, R.A., Bauer, W.F., Harrup, M.K., Allen, C.W., Elayan, A., 2003. On the mechanism of ion transport through polyphosphazene solid polymer electrolytes: NMR, IR, and Raman spectroscopic studies and computational analysis of <sup>15</sup>N-labeled polyphosphazenes. *J. Phys. Chem. B* 107, 3168-3176.

Martínez, L., Andrade, R., Birgin, E., Martínez, J., 2009. Software news and update packmol: a package for building initial configurations for molecular dynamics simulations. *J. Comput. Chem.* 30, 2157-2164.

McQueen, N., Gomes, K.V., McCormick, C., Blumanthal, K., Pisciotta, M., Wilcox, J., 2021. A review of direct air capture (DAC): scaling up commercial technologies and innovating for the future. *Progress in Energy* 3, 032001.

Nelson, M.R., Borkman, R.F., 1998. Ab initio calculations on CO<sub>2</sub> binding to carbonyl groups. *J. Phys. Chem. A* 102, 7860-7863.

Nilkar, A.S., Orme, C.J., Klaehn, J.R., Zhao, H., Adhikari, B., 2023. Life Cycle Assessment of Innovative Carbon Dioxide Selective Membranes from Low Carbon Emission Sources: A Comparative Study. *Membranes* 13, 410.

Ohto, T., Backus, E.H., Hsieh, C.-S., Sulpizi, M., Bonn, M., Nagata, Y., 2015. Lipid carbonyl groups terminate the hydrogen bond network of membrane-bound water. *J. Phys. Chem. Lett* 6, 4499-4503.

Orme, C.J., Klaehn, J.R., Harrup, M.K., Luther, T.A., Peterson, E.S., Stewart, F.F., 2006a. Gas permeability in rubbery polyphosphazene membranes. *Journal of Membrane Science* 280, 175-184.

Orme, C.J., Klaehn, J.R., Harrup, M.K., Luther, T.A., Peterson, E.S., Stewart, F.F., 2006b. Gas permeability in rubbery polyphosphazene membranes. *J. Membr. Sci* 280, 175-184.

Orme, C.J., Klaehn, J.R., Stewart, F.F., 2004. Gas permeability and ideal selectivity of poly [bis-(phenoxy)phosphazene], poly [bis-(4-tert-butylphenoxy)phosphazene], and poly [bis-(3,5-di-tert-butylphenoxy)(1.2)(chloro)(0.8)phosphazene]. *Journal of Membrane Science* 238, 47-55.

Orme, C.J., McNally, J.S., Klaehn, J.R., Stewart, F.F., 2021. Mixed substituent ether-containing polyphosphazene/poly (bis-phenoxyphosphazene) blends as membranes for CO<sub>2</sub> separation from N<sub>2</sub>. *Journal of Applied Polymer Science* 138, 50207.

Park, H.B., Kamcev, J., Robeson, L.M., Elimelech, M., Freeman, B.D., 2017. Maximizing the right stuff: The trade-off between membrane permeability and selectivity. *Science* 356, eaab0530.

Potoff, J.J., Siepmann, J.I., 2001. Vapor-liquid equilibria of mixtures containing alkanes, carbon dioxide, and nitrogen. *AIChE J.* 47, 1676-1682.

Price, D.J., Brooks III, C.L., 2004. A modified TIP3P water potential for simulation with Ewald summation. *J. Chem. Phys* 121, 10096-10103.

Rablen, P.R., Lockman, J.W., Jorgensen, W.L., 1998. Ab initio study of hydrogen-bonded complexes of small organic molecules with water. *J. Phys. Chem. A* 102, 3782-3797.

Rafiq, S., Deng, L., Hägg, M.B., 2016. Role of facilitated transport membranes and composite membranes for efficient CO<sub>2</sub> capture—a review. *ChemBioEng Rev.* 3, 68-85.

Raveendran, P., Wallen, S.L., 2002. Cooperative C–H⋯O Hydrogen Bonding in CO<sub>2</sub>–Lewis Base Complexes: Implications for Solvation in Supercritical CO<sub>2</sub>. *Journal of the American Chemical Society* 124, 12590-12599.

Riboldi, L., Bolland, O., 2017. Overview on Pressure Swing Adsorption (PSA) as CO<sub>2</sub> Capture Technology: State-of-the-Art, Limits and Potentials. *Energy Procedia* 114, 2390-2400.

Robeson, L.M., 2008. The upper bound revisited. *Journal of Membrane Science* 320, 390-400.

Rochelle, G.T., 2012. Thermal degradation of amines for CO<sub>2</sub> capture. *Current Opinion in Chemical Engineering* 1, 183-190.

Sekizkardes, A.K., Budhathoki, S., Zhu, L., Kusuma, V., Tong, Z., McNally, J.S., Steckel, J.A., Yi, S., Hopkinson, D., 2021. Molecular design and fabrication of PIM-1/polyphosphazene blend membranes with high performance for CO<sub>2</sub>/N<sub>2</sub> separation. *Journal of Membrane Science* 640, 119764.

Sergei G. Kazarian, M.F.V., Frank V. Bright, Charles L. Liotta, and Charles A. Eckert, 1996. Specific Intermolecular Interaction of Carbon Dioxide with Polymers. *Journal of the American Chemical Society* 118, 1729-1736.

Siqueira, R.M., Freitas, G.R., Peixoto, H.R., Nascimento, J.F.d., Musse, A.P.S., Torres, A.E.B., Azevedo, D.C.S., Bastos-Neto, M., 2017. Carbon Dioxide Capture by Pressure Swing Adsorption. *Energy Procedia* 114, 2182-2192.

Stewart, F.F., Orme, C.J., Klaehn, J.R., Adhikari, B., Shenderova, O.A., Nunn, N.A., Torelli, M.D., McGuire, G.E., Lee, T.H., Balachandran, U., 2021. Mixed Matrix Membranes, and related gas separation membrane apparatuses, gaseous fluid treatment Systems, and Methods. US Patent App. 17/174,796.

Stickel, J.J., Adhikari, B., Sievers, D.A., Pellegrino, J., 2018. Continuous enzymatic hydrolysis of lignocellulosic biomass in a membrane-reactor system. *Journal of Chemical Technology & Biotechnology* 93, 2181-2190.

Stone, M.L., Rae, C., Stewart, F.F., Wilson, A.D., 2013a. Switchable polarity solvents as draw solutes for forward osmosis. *Desalination* 312, 124-129.

Stone, M.L., Wilson, A.D., Harrup, M.K., Stewart, F.F., 2013b. An initial study of hexavalent phosphazene salts as draw solutes in forward osmosis. *Desalination* 312, 130-136.

Thompson, A.P., Aktulga, H.M., Berger, R., Bolintineanu, D.S., Brown, W.M., Crozier, P.S., in't Veld, P.J., Kohlmeyer, A., Moore, S.G., Nguyen, T.D., 2022a. LAMMPS-a flexible simulation tool for particle-based materials modeling at the atomic, meso, and continuum scales. *Computer Physics Communications* 271, 108171.

Thompson, A.P., Aktulga, H.M., Berger, R., Bolintineanu, D.S., Brown, W.M., Crozier, P.S., in 't Veld, P.J., Kohlmeyer, A., Moore, S.G., Nguyen, T.D., Shan, R., Stevens, M.J., Tranchida, J., Trott, C., Plimpton, S.J., 2022b. LAMMPS - a flexible simulation tool for particle-based materials modeling at the atomic, meso, and continuum scales. *Computer Physics Communications* 271, 108171.

Wang, J., Wang, W., Kollman, P.A., Case, D.A., 2006. Automatic atom type and bond type perception in molecular mechanical calculations. *Journal of Molecular Graphics and Modelling* 25, 247-260.

Wang, J., Wolf, R.M., Caldwell, J.W., Kollman, P.A., Case, D.A., 2004. Development and testing of a general amber force field. *Journal of Computational Chemistry* 25, 1157-1174.

Wang, Y., Balbuena, P.B., 2004. Combined ab initio quantum mechanics and classical molecular dynamics studies of polyphosphazene polymer electrolytes: competitive solvation of Li<sup>+</sup> and LiCF<sub>3</sub>SO<sub>3</sub>. *J. Phys. Chem. B* 108, 15694-15702.

Wang, Z., Xing, A., Shen, H., 2023. Effects of nitrogen addition on the combined global warming potential of three major soil greenhouse gases: A global meta-analysis. *Environmental Pollution*, 121848.

Wendt, D.S., Adhikari, B., Orme, C.J., Wilson, A.D., 2016. Produced Water Treatment Using the Switchable Polarity Solvent Forward Osmosis (SPS FO) Desalination Process: Preliminary Engineering Design Basis, Geothermal Resources Council Meetings. Geothermal Resources Council, San Francisco, CA.

Wendt, L.M., Wahlen, B.D., Adhikari, B., 2022. Methods of producing succinic acid from a biomass. US Patent App. 17/652,835.

Wilson, A.D., Orme, C.J., Klaehn, J.R., Adhikari, B., Stewart, F.F., Snyder, S.W., 2021. Methods, systems, and apparatuses for treating fluids using thermal gradient osmosis. US Patent App. 17/009,360.

Wilson, A.D., Stewart, F.F., 2013. Deriving osmotic pressures of draw solutes used in osmotically driven membrane processes. *Journal of Membrane Science* 431, 205-211.

Wilson, A.D., Wendt, D.S., Orme, C.J., Adhikari, B., Ginosar, D.M., 2022. Methods and systems for treating an aqueous solution. US Patent 11,261,111.

Wilson, A.D., Wendt, D.S., Orme, C.J., Mines, G.L., Jones, M.G., Adhikari, B., 2019. Methods and systems for treating a switchable polarity material, and related methods of liquid treatment. US Patent 10,195,543.

Yin, J., Zhang, J., Wang, C., Lv, N., Jiang, W., Liu, H., Li, H., Zhu, W., Li, H., Ji, H., 2021. Theoretical insights into CO<sub>2</sub>/N<sub>2</sub> selectivity of the porous ionic liquids constructed by ion-dipole interactions. *Journal of Molecular Liquids* 344, 117676.

Yu, C.-H., Huang, C.-H., Tan, C.-S., 2012. A Review of CO<sub>2</sub> Capture by Absorption and Adsorption. *Aerosol and Air Quality Research* 12, 745-769.

Zhao, J., Deng, S., Zhao, L., Yuan, X., Wang, B., Chen, L., Wu, K., 2021. Synergistic and competitive effect of H<sub>2</sub>O on CO<sub>2</sub> adsorption capture: Mechanism explanations based on molecular dynamic simulation. *Journal of CO<sub>2</sub> Utilization* 52, 101662.

Zhu, J., Baker, S.N., 2014. Lewis base polymers for modifying sorption and regeneration abilities of amine-based carbon dioxide capture materials. *ACS Sustainable Chem. Eng.* 2, 2666-2674.